Materials Research Bulletin 160 (2023) 112133

Contents lists available at ScienceDirect

Materials Research Bulletin

journal homepage: www.elsevier.com/locate/matresbu

Research Papers

Tungsten oxysulfide nanoparticles interspersed nylon based e-textile as a low cost, wearable multifunctional platform for ultra-sensitive tactile sensing and breath sensing applications

Sushmitha Veeralingam, Abhishek Gandrothula, Sushmee Badhulika *

Department of Electrical Engineering, Indian Institute of Technology Hyderabad, Kandi, NH-9, Sangareddy, Hyderabad, Telangana 502285, India

ARTICLE INFO

Keywords:
Nylon
Tungsten oxysulfide ($WS_2|O$)
Breath monitoring
Gesture monitoring
Pressure detection

ABSTRACT

In this work, we report the hydrothermal synthesis of Tungsten Oxysulfide ($WS_2|O$) nanoparticles interspersed onto porous, lightweight Nylon fabric as a clean-room-free, multifunctional sensor for detection of human breath, strain, and pressure. Morphological characterizations reveal the uniform dispersion of the conductive $WS_2|O$ nanosheets across the ultra-thin fibers of nylon. The fabricated $WS_2|O$@nylon-based device as a breath sensor exhibits excellent sensitivity towards different breath patterns. The optimization studies resulted in a 4-layered high-performance piezoresistive wearable pressure sensor. It exhibited a sensitivity of 1.5 kPa^{-1}, response time of 0.2 sec over a dynamic range of 50 Pa to 350 Pa. A Gauge factor of 24.2 and good mechanical stability across 10,000 cycles of compressive strain exhibited by the strain sensor makes it suitable for gesture recognition. The exceptional sensitivity, stability with good flexibility prove it as a promising device platform for the development of various wearable multifunctional sensor applications.

1. Introduction

Sensors that are flexible, adaptable, and portable are becoming increasingly popular for monitoring various body parameters due to their ease of integration with the human body [1]. Wearable sensors with skin-friendly cloth-based substrates can be easily integrated on the human skin thus being able to perfectly monitor the physical stimuli without creating any discomfort to the people [2–4]. Adaptable and versatile sensors are made to monitor human activity and also, they are used as a mode of communication for physically disabled persons [5]. Wearable and flexible strain sensors are gaining popularity due to their broad usage in soft robotics [6,7], health care, touch-on screen, electronic skin, and sensors. The multi-functional sensing ability to recognise both physical and chemical stimuli enhances the advantage of the sensor by reducing the requirement of multiple sensors for the monitoring of activities and also helps in healthcare monitoring for the detection of various diseases [8,9]. The three fundamental transduction mechanisms namely piezoelectric, capacitive, piezoresistive are helpful in converting the physical stimuli like pressure and strain into a response that can be easily captured and monitored [10]. However, due to their low cost, simple structure, great sensitivity, and ease of signal collecting, piezoresistive sensors have gained prominence [11]. The stimuli upon the piezoresistive sensor affects the size and shape of the device and thus the exerted pressure/strain is reflected in the variability of resistance of the device. However, the wearable devices with planar, in-compressible substrates, complex fabrication techniques limit their potential to be adaptive. Therefore, it is interesting to explore new sensors by combining unconventional, flexible substrates and novel nano-materials for the development of multi-functional sensors.

Most of the flexible sensors are fabricated by using polydimethylsiloxane, Indium Tin Oxide as substrates [12–15]. Even though they possess scalability and compatibility, detecting subtle pressures and mounting them on the human body seems challenging. Therefore, the correct choice of substrate and the nano-material that suits well with our applications plays main role in magnifying the usage of the sensor. So to overcome this, melamine foam, nylon fabric, spacer fabric are used as substrates because of their compressible nature, large surface area and porosity [16,17]. Recently, various cloth substrates are explored to make the device light, flexible and simpler to assemble with the human body. The porous nature, the range of temperature, mechanical stability and the good surface area makes the nylon cloth feasible to use as the substrate. When compared to cotton and spacer fabric, tear-resistant

* Corresponding author.
E-mail address: sbadh@iith.ac.in (S. Badhulika).

https://doi.org/10.1016/j.materresbull.2022.112133
Received 13 June 2022; Received in revised form 1 December 2022; Accepted 18 December 2022
Available online 20 December 2022

property and the lightweight nature of nylon fabric gives an added advantage of durability and provides facility to be integrated on human skin comfortably. The pure nylon fabric alone is non-conductive and therefore it has to be enhanced with some conductive material.

There is a wide variety of available conductive/semiconductive nanomaterials that have been used as the receptor or the active compound in sensing applications. In this regard transition metal dichalcogenides (TMDCs, MX_2 (M= W, Mo, Sn; X= S, Se, Te) e.g., MoS_2, WS_2, $MoSe_2$, SnS_2) which have special 2D layered structures is an appropriate choice for the effective sensing of stimuli. The Surface-to-Volume ratio, the atomic-level thickness and exceptional electronic properties of TMDCs rises their prominence to a higher level in multi-functional sensing applications [18].

Tungsten Disulphide (WS_2; a TMDC with M=W, X=S) is a good option for the sensing activity because of its suitable bandgap and absorption-free energy at low-level temperatures [19,20]. This material crystallises in a 2D structure where the metallic atom (M = W) is covalently bonded to 6 chalcogen neighbours (X = S) inside the X-M-X layers. It is noteworthy to mention that, TMDC materials with layer-dependent properties have been considered as promising gas-sensing materials because they exhibit sensitivity and stability in the atmospheric environment and a significant response due to its high surface-to-volume ratio. that are useful for strain and pressure applications. The layers are stacked along the c-axis, with weak van der Walls forces connecting them by which we can experience layer-dependent tuneable electrical properties and abundant active edge sites that will help the device react to both physical and chemical stimuli [21,22]. Reports show that non-metallic doping of WS_2 adds the properties of physisorption and chemisorption to the material which plays a key role in enhancing the chemical stimuli sensing activity [23,24]. Among the non-metal elements oxygen gets high priority due to its high electronegativity and being in the same group of sulphur in the periodic table, it gives more ability to the sensor to respond to the chemical stimuli.

In this paper, $WS_2|O$ interspersed nylon fabric device for multifunctional sensory applications is fabricated by using low-cost precursors and a facile hydrothermal method. The fabricated $WS_2|O$ coated nylon sensor is used as a breath, strain, and pressure sensor due to its inspiring flexible and conductive nature. The morphological studies show the stacked up nanosheet structures of $WS_2|O$ and also reveal the interspersion of $WS_2|O$ molecules on the nylon fibers. The fabricated breath sensor is sensitive to human breath thereby capable of constantly monitoring a healthy human's breath. It is also able to differentiate the intensity and frequency of breaths which can be useful for medical purposes. The fabricated strain sensor shows an appreciable Gauge Factor (GF) when compared to other similar devices [17,25]. The strain sensor is able to monitor human movement by attaching the device to the various body parts thus giving us the platform for gesture recognition. The pressure sensor is able to sense a wide dynamic range of pressure. The response and recovery times are found to be low when compared to other similarly reported multifunctional devices [26]. The pressure sensor is even able to detect the plantar pressure i.e., pressure caused by our body parts also used for weight tracking of light-weight objects which makes the device suitable to use in the practical scenario. Textile substrates hold huge potential as it allows contact between the sensor and the body, and have good mechanical strength, softness, and stretchability, while their extensive surface area enables the convenient integration of the associated electronic components. However, the previously reported textile-based sensors were associated with several challenges in achieving high linearity and cycling stability. In this work, Tungsten Oxysulfide (WS2|O) nanoparticles interspersed with lightweight Nylon fabric exhibited excellent linearity and cyclic stability of 10,000 bending cycles. This is, to the best of the author's knowledge, the first report on $WS_2|O$ and nylon-based e-textile for multi-functional wearable applications.

2. Experimental details

2.1. Materials and equipment

Tungsten chloride (WCl_6 - M.W:- 396.61 g/mol, 99%), Thioacetamide (C_2H_5NS - M.W:- 75.13 g/mol, 99%) are acquired from Sigma Aldrich and utilised without further refining. Nylon-6 (pore size -100nm) cloth is bought from a supermarket and used as the substrate. Ethanol (purity:- 99%) is purchased from Changshu Hongsheng Fine Chemical Co. Ltd. DI water is procured from a Millipore setup (Merck, Direct Q 3-UV). Finolex copper wires are purchased from supermarket and are used to make contacts.

For the study of surface morphology & topography, Scanning Electroscopy Microscopic analysis is performed by using ZEISS Ultra-55 SEM. Xpert PRO X-Ray Diffractometer (XRD) using Cu-Kα radiation is utilised for the structural characterisation investigations. Transmission Electron Microscopy (JEOL JEM 2100FX TEM) is done to investigate the morphology and crystalline structure of $WS_2|O$. UV- Visible spectroscopy (SL 210 UV VIS Spectrophotometer) and PL-Spectroscopy are done for the examination of absorbance spectra and the band gap of $WS_2|O$. All the electrical measurements are done using Keithley 2450 Smu Simulator.

2.2. Synthesis of $WS_2|O$ nanosheets

$WS_2|O$ nanosheets are synthesized via hydrothermal technique. First, 100 mM of Tungsten chloride and 1.5 M of Thioacetamide are uniformly mixed in 40 ml of DI water. The solution is stirred at room temperature for 4 hours. Once the compounds are dissolved, a bluish-grey solution is obtained. Then the solution is transferred into a 50ml Teflon-Coated autoclave and preserved at 265°C for 24 hours. Then the autoclave is allowed to settle down to room temperature, and the resultant sample is separated by centrifugation. The extracted sample is washed few times with Ethanol and DI Water, then kept to dry in vacuum at 70°C for 5 hours. Fig. 1(a) depicts the entire synthesis process.

2.3. Fabrication of the sensor

Initially, the Nylon cloth (substrate) is prepared by cleaning it multiple times with DI water and drying it for 4 hours. And then 80 mg of $WS_2|O$ powder is mixed evenly in 10 ml of DI water under ultrasonication.

2.3.1. Breath sensor

The as-prepared nylon cloth is cut into 1 cm X 1 cm dimensions and the prepared solution is drop cast onto the substrate and kept at 70°C for drying for 10 minutes. The process of drop casting and drying is repeated 5 times to ensure sample uniformity. Later the contacts are taken out using conductive Ag paste and copper wires.

2.3.2. Strain sensor

The as-prepared nylon cloth is cut into 2 cm X 1 cm dimensions and the prepared solution is drop cast onto the substrate and it is maintained at 70°C for drying. Three such coated and dried cloths are stacked upon each other and the contacts are taken from both sides by using conductive Ag paste and copper wires.

2.3.3. Pressure sensor

The as-prepared nylon cloth is cut into 4 cm X 1 cm dimensions and the prepared $WS_2|O$ solution is drop casted onto the substrate and it is dried at 70°C. Four such coated cloths are stacked upon each other. Similarly the contacts are made by silver paste and copper wires. The region between the contacts is used as the active region where we can apply pressure. The fabrication process is shown in Fig. 1(b).

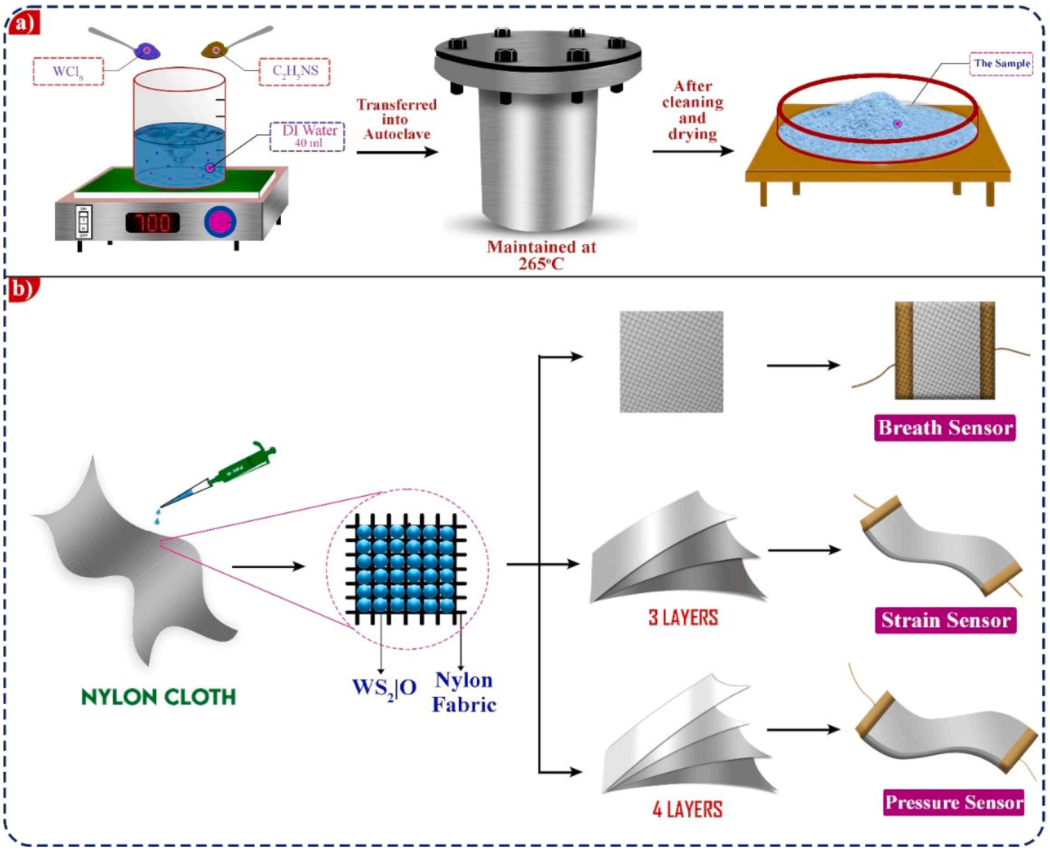

Fig. 1. (a) Schematic showing the synthesis of $WS_2|O$; (b) Schematic describing the fabrication of breath, strain and pressure sensor.

3. Results and discussion

3.1. Morphological studies

The as-synthesized $WS_2|O$ is studied via FESEM and TEM analysis. Fig. 2(a) portrays the low magnification FESEM micrograph of $WS_2|O$ decorated fibrous nylon cloth. The fibers of the nylon cloth are observed to be closely aligned with each other. This serves as a porous decorating template for uniform growth of $WS_2|O$ nanoparticles. The pore size is suitable enough for breathing. The high-magnification FESEM images of the coated nylon cloth are displayed in Fig. 2(b), 2(c). From Fig. 2(b) the width of the fibre is measured and it is found to be 55.8 μm. In Fig. 2(c) the $WS_2|O$ crystals were uniformly distributed on the surface of the nylon fibers. Those crystals are interspersed on the threads of the nylon cloth and they are closely connected thus making the entire surface (cloth) as conductive. The interaction between $WS_2|O$ and nylon can be attributed to the absorbing of the solution by the nylon cloth during drop casting. Fig. 2(d) further depicts the nanostructure of the $WS_2|O$ material.

TEM analysis is performed to examine the structural morphology of $WS_2|O$. Fig. (2e), (2f) depicts the high magnification TEM images of $WS_2|O$. Fig. 2(e) clearly shows the stacked up nanosheets of $WS_2|O$. Another perspective of high-magnified TEM image shown in Fig. 2(f) also reveals the nanosheet structure of the material confirming the uniformity of structure of the material. TEM images were also used to identify the average length of the $WS_2|O$ nanosheets as shown in SI Fig. S1. The gaussian normalization process was carried out by measuring the length of all the nanosheets present in the TEM image. The average length of the nanosheets was calculated to be 75 ± 3 nm from the normalized gaussian fit curves, as shown in Fig. b. The minimum length and the maximum length were obtained as 51 and 98 nm, respectively. The inter-lattice spacings of the compound are also captured in Fig. 2(g) and the spacing is found to be 0.350 nm. The Selected area electron diffraction (SAED) pattern is observed in Fig. 2 (h). The EDS elemental mapping is performed and the results can be seen in Fig. 2(i), 2(j), 2(k). The compound contains tungsten in high amount, sulphur and also the oxygen which confirms our compound being Tungsten Oxysulfide ($WS_2|O$) The oxygen atoms are present in our compound as a result of doping that is done while synthesizing. The 1:15 molar ratio of the tungsten to sulphur source helps us in doping the oxygen atoms [24].

Further, the crystalline structure of Tungsten Oxysulfide nanosheets is investigated using XRD with the CuKα radiation (1.54 Å). The results exhibited the formation of high intense sharp peaks which denotes the crystalline nature of the material. Fig. 3(a) displays the diffraction peaks at 2*theta angles 13.92, 32.67, 49.54, 63.43, 72.08 which denotes the family of crystal planes (002), (101), (103), (105), (112), (203) corresponding to Hexagonal WS_2 (referring to JCPDS #00-002-0131). However additional peaks are also formed at 2*theta angles 23.4, 28.08, 33.93, 52.87, 55.75 corresponding to the crystal planes (010), (106), (116), (2 1 11), (-5 0 11) as a result of the existence of monoclinic WO_3. This is also validated by comparing them to the JCPDS #00-005-0386 standard values.

The absorbance spectra of $WS_2|O$ is examined using UV-VIS spectroscopy. The wavelength of the incident light is made to vary from 150 nm to 800 nm and the graph is plotted between absorbance of the sample and the wavelength of light. Fig. 3(b) shows the obtained absorbance spectra of $WS_2|O$. The absorbance of our compound is found to be prominent in the UV and visible regions. The correlation between absorption coefficient and the photon energy of the synthesized $WS_2|O$ nanosheets is evaluated using Tauc's plot, which is drawn between $(\alpha h\nu)^{1/2}$ and $(h\nu)$, where 'α' denotes the absorption coefficient, 'h' is the Planck's constant, and 'ν' indicates the frequency. The bandgap is calculated to be 2.81 eV from the Tauc's plot as shown in Fig. 3(c). The

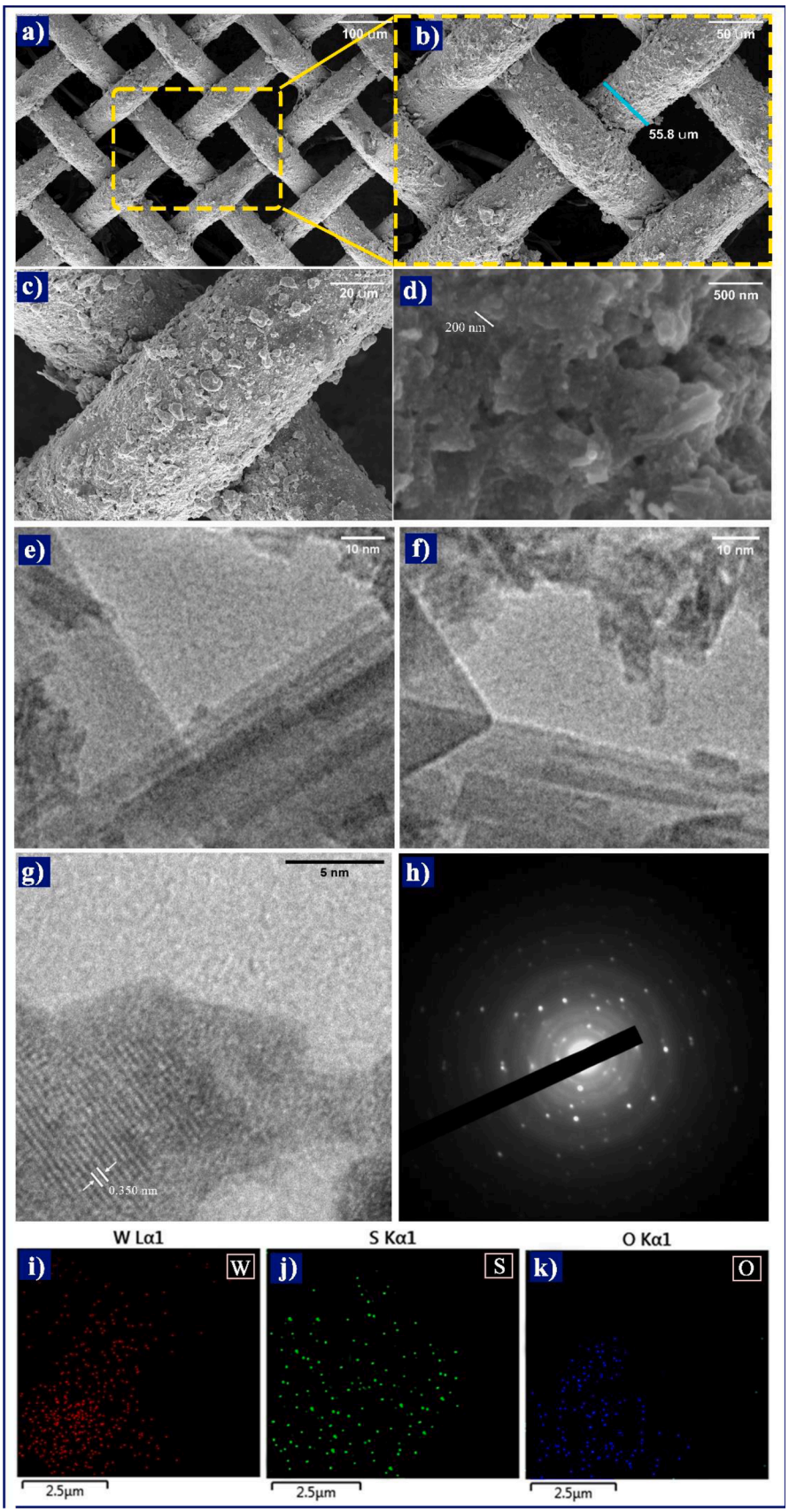

Fig. 2. (a) SEM micrograph of WS_2|O coated nylon cloth; (b) Low magnification SEM image of WS_2|O coated nylon cloth; (c,d) High magnification SEM images of WS_2|O coated nylon cloth; (e,f) High magnification TEM image of WS_2|O; (g) High magnification TEM image of WS_2|O showing inter lattice spacings; (h) SAED pattern of WS_2|O; (i-k) EDS elemental mapping of WS_2|O.

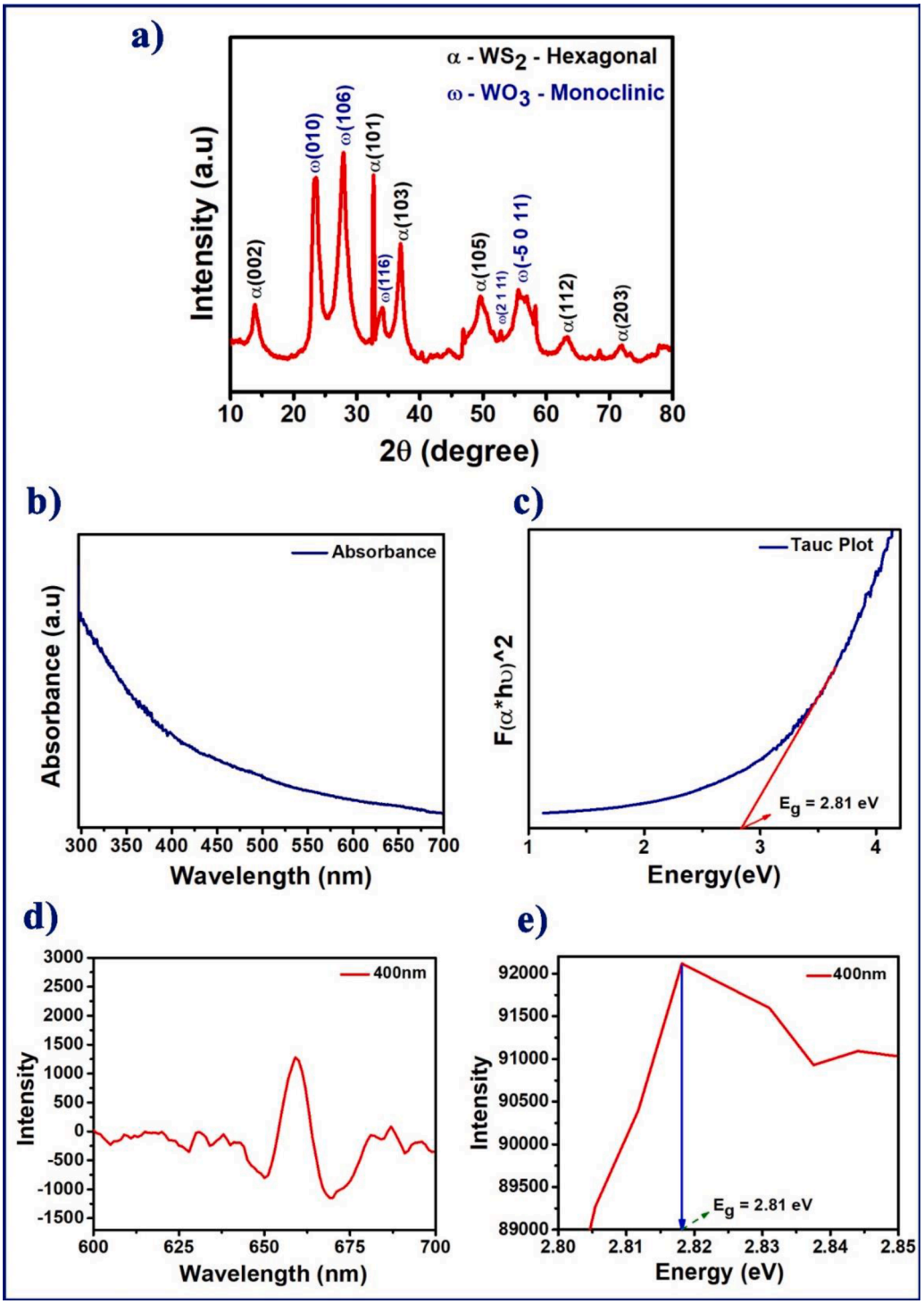

Fig. 3. (a) XRD pattern of $WS_2|O$; (b) Absorbance spectra; (c) Tauc's plot; (d) Photo Luminescence Spectroscopy of $WS_2|O$, (e) Intensity vs Energy plot obtained from PL Spectroscopy.

photoluminescence studies of $WS_2|O$ are also conducted. The excitation wavelength used is 400 nm. It is taken from the absorbance range determined by UV–vis spectroscopy. The obtained PL results are shown in Fig. 3(d) and 3(e). The $WS_2|O$ demonstrates a wide peak around 2.81 eV at 400 nm excitation.

3.2. Breath sensing

Human breath has been considered as an important biomarker to diagnose lung-related diseases like asthma, lung cancer, pneumonia related to breath, and even Parkinson's disease [27–29]. For most of these diseases which don't have any alarming symptoms at their initial stages, the troublesome breath can act as a mild sign which when detected at the early stage gives a chance for a better diagnosis.

A variety of conductive compounds and substrates have been used to fabricate effective and responsive breath sensors. Among them, the lightweight and human-body adaptable textile-based substrates: Cotton, Nylon, and Paper are chosen and optimization studies are performed. The details can be seen in Section S1 in the supplementary information. And those studies resulted in finalising the nylon cloth because of its

excellent porosity and tear-resistant property which helps in breath, strain and pressure sensing applications. The fibre alignment of the nylon cloth helps in holding the conductive $WS_2|O$ particles thus making the entire cloth (substrate) conductive. So the nylon cloth is chosen out of them to be used as the substrate and the device is fabricated as mentioned in Section 2.

And that $WS_2|O$@nylon device is fixed to a face mask by a biocompatible polyimide tape, and human breath is examined. A voltage of 0.1 V is supplied externally to the fabricated device and the nasal breath of a 24-year-old male is monitored for 30 seconds. The corresponding response toward exhalation and inhalation cycles is estimated and displayed in Fig. 4(a). The magnified part of Fig. 4(a) is shown in Fig. 4(b) where the rise in peak during exhalation and fall in peak during inhalation is observed. From these figures, it is depicted that during the exhalation process the resistance of the sensor decreases and the current increases, and during inhalation, the current decreases gradually to its original value. Thus a peak of the current counts a breath. In this way, the breath per minute (BPM) can be calculated, and here for 30 seconds, the number of breaths is found to be 11.

Usually, the exhaled breath contains water vapor, so the H_2O molecules when imparted on the sensor's active region, they experience a strong electric field and due to that, the H_2O molecules divide into H_3O^+ ions and electrons. Those electrons under the existing electric field get drifted across the sensor through the Cu wires attached and increases the output current. The variation in water molecule concentration during respiration modulates the response of the breath sensor and accordingly the breath patterns are tracked [2].

In general, humans breathe through their mouths seldomly. If air

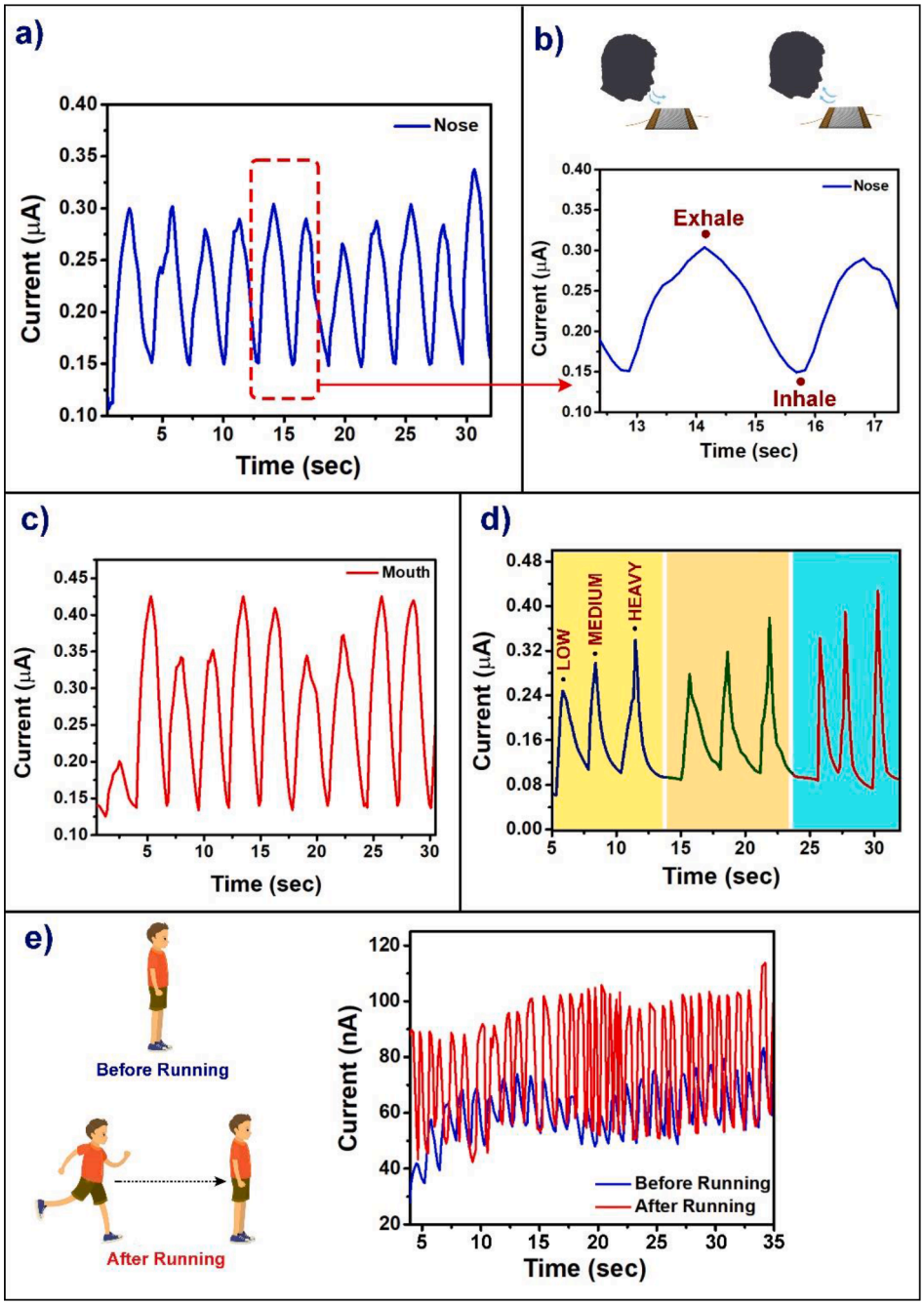

Fig. 4. Breath Sensing (a) Temporal response for nasal breathing, (b) Magnified image of figure a for detailed exhalation and inhalation process, (c) Temporal response for oral breathing, (d) Breathing cycle studies for three different intensities, (e) Monitoring of human breath before and after running.

enters the respiratory tract without being filtered by the nose, then dust, germs, and even PM 2.5 particles can easily obstruct the air tract, leading to bronchitis and other lung disorders [30]. So, it's required to monitor and distinguish the oral breathing from the nasal breathing. And the response obtained for the oral breathing is shown in Fig. 4(c). We can clearly see that the peaks have more magnitude in the case of oral breathing than that of nasal respiration. As the amount of vapor exhaled during oral breathing is more when compared to that of nasal, relatively a large number of ions and electrons are produced which yields high output current [30]. The active edge sites of WS_2|O help in absorbing the H_2O molecules exerted during exhalation [22]. The oxygen doped in WS_2 enhances the capturing of water molecules due to its high electronegativity. Consequently, the sensing ability is improved. And during inhalation, the water molecules start to get desorbed off the surface and gradually the current tends to decrease. It should be observed that the desorption process is delayed, because the exhaled

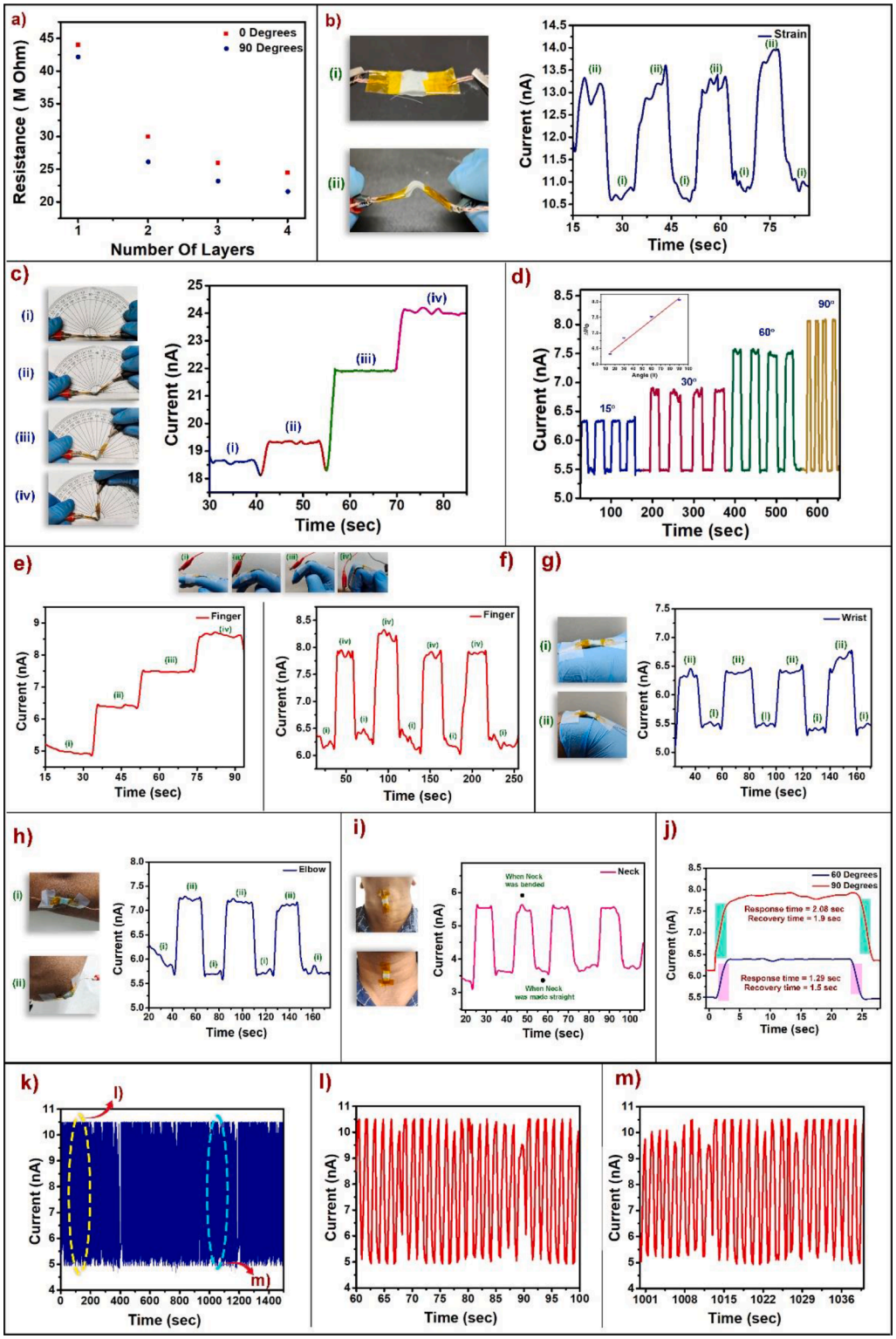

Fig. 5. Strain Sensing (a) Resistance vs number of layers graph with and without bending; (b) Temporal response towards tensile and compressive strain; (c) 0^o – 90^o Angular strain response of the strain sensor; (d) Temporal response of 15–90^o strain and inset: calibration plot; (e,f) The response based on the movement of Finger; (g–i) The response based on the bending of wrist, elbow and neck respectively; (j) Response and Recovery time for 60^o and 90^o strain; (k) Response of the strain sensor for compressive and tensile strain for 1500 cycles, (b) Magnified version of 6k from 60 to 100 s, (c) Magnified version of 6k from 1000 to 1040 s.

water molecules from breath are trapped in the interlayer threads of the nylon cloth and also penetrate into the $WS_2|O$ nanocrystals, thereby taking time to get desorbed. The large surface area of the device plays a role in capturing the exhaled molecules.

3.2.1. Applications of breath sensor

To test the sensor for real-time applications, the fabricated breath sensor is also checked for the various conditions of breath as a function of its intensity i.e., normal breathing, moderate breathing and heavy breathing. The obtained results are shown in Fig. 4(d) and the difference in the magnitude of peaks can be clearly observed. Three different intensities of breath for three cycles is monitored and the device is found to track the breath. The same pattern observed in the results confirms the repeatability of the device. This action can be attributed to the amount of vapor exhaled under these three conditions. High number of H_2O molecules diffused into the surface of the sensor yields high number of H_3O^+ ions and electrons as a result of which the output current is increased.

The practical application of the fabricated breath sensor is further investigated by examining the frequency of the breath before and after a moderate exercise. It is observed that the frequency of peaks and the magnitude of the response is higher just after the exercise when compared to that of normal condition (i.e. before exercise). The obtained results are shown in Fig. 4(e). The peaks before exercise are found to be 26 whereas, after exercise, they are found to be 35. In the post-exercise condition, the absorption and desorption processes of H_2O molecules on the nylon cloth occurs more rapidly than in normal conditions, so rise and fall in current happen immediately thus increasing the frequency of the output. The difference between the intensities of the exhaled breath under these two conditions reflects in the difference of magnitude of responses. The capability of detecting wide range of frequencies and magnitudes of breath helps the device to be employed for the breath-monitoring of patients suffering from breathing problems. The response of the breath sensor towards interfering species was also performed and is given in SI Section S5.

3.3. Strain sensing

The flexible nature, robustness, and conductivity of the $WS_2|O$@nylon device makes it useful for strain-sensing applications. The $WS_2|O$ coated nylon cloth is cut into 2 cm X 1 cm dimensions and the layer-optimization studies are done by stacking few layers of such 2×1 $WS_2|O$@nylon cloths and measuring its resistance. The corresponding results of resistance vs number of layers stacked can be seen in Fig. 5(a). The resistance value of the device with three layers is 25 ± 2 M Ohms, and with four layers is 23 ± 2 M Ohms, where the difference is very minimal. Also, with the increase in the number of layers i.e., 5 layers and 6 layers, the resistance value was found to remain 22 ± 3 M ohms and 23 ± 2 M ohms, respectively [data not shown]. The change in resistance was found to saturate with the increase in the number of layers. The device is tested by applying tensile and compressive strains i.e. stretching and compressing the device along its length. The stretching and compressing of the device are done using a customized technographic TGI setup. The device is tested by applying automated tensile and compressive strains i.e., stretching and compressing the device along its length using a tensile and compression testing machine. The response is observed by applying a voltage of 0.5 V and the corresponding results are shown in Fig. 5(b). When the device is compressed, there is an increase in current and again, when the device is restored to the tensile state the response also sets back rapidly to the previous value. When the device is compressed the conductive $WS_2|O$ molecules throughout the layers overlap with each other and make a better conductive path for the electrons to travel across the device and the resistance gets decreased. And once again when the device is set back to its normal state, the $WS_2|O$ molecules stop overlapping thus the resistance increases to its previous value. This indicates that the device can recognize and differentiate tensile and compressive strains. The device is again tested to check the angular strain, the device is bent at multiple angles and the responses are recorded and displayed in Fig. 5(c). The current started to increase as we increase the angle of bending from 0 degrees to 90 degrees. Uniform current is maintained when the device is positioned at a certain angle and once the device is subjected to more angular strain then the shifting of the current level is done and again the new current value is maintained giving the beautiful characteristics required for any real-time application. The current value clearly follows the angle of the strain applied. As we increase the angle of bending, the conductive $WS_2|O$ molecules come closer to each other and thereby decreasing the resistance of the device. The temporal response is performed on the device and the results are presented in Fig. 5(d). The device is subjected to increasing-angular strain for multiple cycles. The sensor displayed a rise in current when strain is applied and a drop in current once the sensor is restored to its normal position. The uniform cycles of response for application of certain strain can also be seen, thus announcing the repeatability property of the device. The Gauge factor (GF) denotes the ratio of fractional change in resistance to the change in the strain applied. The gauge factor of the strain sensor is found to be 24 upon application of an external strain of 60 degrees. For higher strain levels, the sensor exhibited a further rise in current, which can be attributed to the establishment of $WS_2|O$ contacts across the layers. The inset of Fig. 5(d) shows the calibration plot indicating the linear response of the strain sensor

To test it for real-time applications the device is attached to the finger and the finger is made to move and the corresponding results are shown in Fig. 5(e). The movement of the finger is easily tracked based on the magnitude of the current. The sustainability test is also done to check whether the device is able to restore to its normal current value. That report can be seen in Fig. 5(f). Similarly, the tracking of the wrist, elbow, and even neck are monitored and the results are seen in Fig. 5(g), Fig. 5 (h) and Fig. 5(i) respectively. From this, we can efficiently use the device to track human gestures which can be a help to physically handicapped persons. The device attached to the knee can also be used to track the human motion and many more ways for this device to elaborate it's wings in the sensor world. The response and recovery time which plays a key role in real-time applications are also measured and found to be 1.29 sec and 1.5 sec respectively at 60 degrees angular strain and 2.08 sec and 1.9 sec respectively at 90 degrees angular strain. The corresponding data is shown in Fig. 5(j).

3.3.1. Flexibility and repeatability tests

The fabricated strain sensor is tested for repeatability by applying the same continuous compressive and tensile strain over 1500 cycles. The obtained response is illustrated in Fig. 5(k). Excellent repeatability can be observed throughout 1500 cycles. Fig. 5(l) shows the magnified response from 60 to 100 seconds and Fig. 5(m) shows the magnified graph from 1000 to 1040 seconds. The response of the strain sensor for 10,000 loading and unloading cycles was performed, and the corresponding response is given in Fig. S3. These figures demonstrate the remarkable repeatability with only a minute deviation in the normalized response over a small range of bending cycles. The strain sensor's achieved repeatability can be ascribed to the robustness of $WS_2|O$ nanosheets which are closely and strongly stacked together. The flexible and tear-resistant property of nylon fabric also aids the repeatability property of the strain sensor.

3.4. Pressure sensor

Wearable fabric-based pressure sensors owing to their flexibility and simplicity, are a great technique to monitor human body movements based on the force exerted on the sensor thus having wide applications in biological monitoring and human-machine interface [31].

The flexible and tactile nature of the nylon fabric in addition to the stacked-up layers of $WS_2|O$ nanosheets aids the pressure-sensing

capabilities of the device. The resistance value of the device with four layers is 22 ± 2 M Ohms, and with six layers is 17 ±2 M Ohms, where the difference in resistance is very minimal. Also, with the increase in the number of layers i.e., 5 layers and 6 layers, the change in resistance was found to saturate with the increase in the number of layers. The obtained resistance vs layers data can be seen in Fig. 6(a). Pressure applied to the device will help the layers to come into contact and once the pressure is released, the flexible nature of nylon helps the device to reach its normal position. It should be noted that the layers (of 4 cm X 1 cm dimensions) used here are wider when compared to the strain sensor as we need a large contact area for the sensing of pressure. A potential of 0.5V is supplied to the pressure sensor, and the corresponding variability in current is examined by applying various pressures. The temporal response for 6 different pressure values, ranging from 50 Pa to 350 Pa is obtained and displayed in Fig. 6(b). The sensitivity of the pressure sensor is measured as the smallest variation in pressure that can cause a change in the output resistance (i.e., $(\Delta R/R_0)/\Delta P$). The sensitivity of the pressure sensor was measured in the range of 50 Pa to 150 Pa as 1.5 kPa^{-1}. Different current values are recorded for different levels of pressure subjected to the device. The calibration plot is shown in Fig. 6

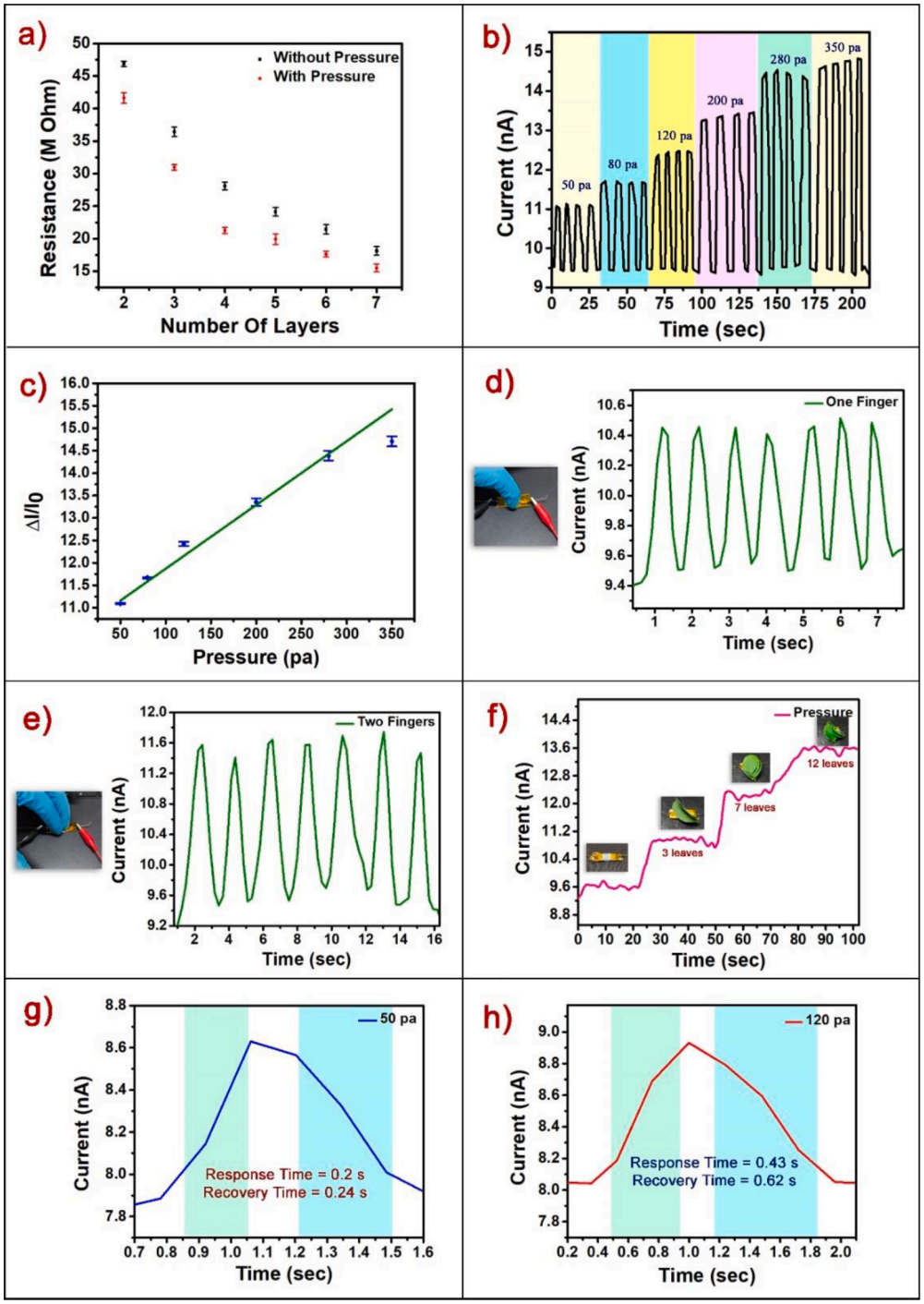

Fig. 6. Pressure Sensing (a) Resistance vs Number of layers stacked, (b) Temporal response for an external pressure of 50 Pa, 80 Pa, 120 Pa, 200 Pa, 280 Pa and 350 Pa; (c) Corresponding Calibration plot; (d,e) Temporal response for a gentle touch of one finger and two fingers respectively; (f) I vs t response for pressure caused by leaves, (g,h) Response and recovery time for 50 Pa and 120 Pa pressure respectively.

(c). The current increases when pressure is applied and once pressure is withdrawn, the current returns to the initial value and this cycle repeats. The increase in current for the applied pressure can be ascribed to the establishment of $WS_2|O$ contacts throughout the device, promoting electron flow across the terminals. The contacts are established between $WS_2|O$ nanosheets, when four layers of nylon fabric get in contact with each other due to the applied pressure, which results in an increase of current throughout the device.

To evaluate the practical applicability of the sensor, it is made to respond to the gentle touch caused by a single finger and two fingers. The results obtained are shown in Fig. 6(d), 6(e) respectively. Higher response is observed for the pressure by two fingers when compared to that of single finger. More pressure leads to more surface area of nylon layers coming into contact and as a result, the formation of temporary contacts between the $WS_2|O$ nanosheets occurs. The device is also tested for the measurement of weight, for which the response is examined for four different cases, a normal device without any pressure, 3 leaves placed on the device, 7 leaves placed on the device, and 12 leaves placed on the device. The data is shown in Fig. 6(f). The excellent response of current, tracking the weight is recorded. The difference between the weight caused by 4-5 leaves is also easily measured and thereby this sensor can be used in weighing light weight objects in the range of 2 – 10 gms.

The response and recovery times for applied pressure of 50 Pa and 120 Pa are measured and displayed in Fig. 6(g), Fig. 6(h) respectively. The response time is the time interval of the response between 10% and 90% of its steady state values. The recovery time is the time required for the response to return to 90% of its initial value once the stimuli is released [32]. Response time and recovery time are found to be 0.2 sec and 0.24 sec for 50 Pa pressure, and 0.43 sec and 0.62 sec for 120 Pa pressure respectively. Increase in pressure leads to establishment of more temporary contacts among the $WS_2|O$ nanosheets, and correspondingly the time for formation of those contacts also increases which results in high response time. Similarly when the pressure is released, since more contacts are previously formed the time for the established contacts to get back to their original state also increases. So increase in pressure leads to increase in response and recovery time. The flexible nature of the nylon enhanced the rapid sensing activity.

Table 1 shows the comparison of the as-fabricated $WS_2|O$ Nylon device with recently reported similar multifunctional and wearable devices. Few reports [14,17] mentioned here use sophisticated and expensive fabrication techniques like sputtering, and knitting and sputtering for the fabrication of the sensor. Furthermore devices like PPy/SR, PPy/β-FeOOH@Nylon [16,35] have only one application whereas some other devices [14,25,34] are limited to two applications i.e. strain and pressure sensing. only two devices [15,17] are used for more than two applications rather than measuring pressure and strain, thus enhancing the usage in the field of multi-functional sensors. There is a mention of few other devices which employed inexpensive fabrication techniques like spin coating and ultra-sonicating, but those devices showed less sensitivity and gauge factor thus limiting their applications in multifunctional wearable sensors [15,35]. In sharp contrast in this work $WS_2|O$ coated light-weight flexible Nylon fabric-based multifunctional sensor is fabricated using a low-cost and facile hydrothermal technique and used for breath, strain and pressure sensing applications. The drop-casted conductive $WS_2|O$ nanosheets are able to be interfaced with the entire nylon fabric thus making the cloth conductive. The flexible and porous nature of nylon allows us to sense the physical and chemical stimuli with the utmost sensitivity. The device also displayed a good gauge factor and sensitivity and moreover it can be fabricated in a clean-room-free environment, thereby making this device promising for developing multifunctional sensors in wearable electronics applications. The cost of the sensor is calculated to be around $1.1 (the complete details can be seen in supplementary information Section S2).

4. Conclusion

In summary, we demonstrated a multi-functional sensor based upon the flexible nylon fabric interspersed with conductive $WS_2|O$ which is used for sensing three different stimuli namely breath, pressure and strain. The device exhibited excellent performance towards each of the stimuli and is further taken for wearable applications namely breath pattern monitoring system, skin-inspired finger touch system and gesture recognition. The device showed good response and recovery time with an excellent gauge factor and remarkable sensitivity thereby making it a promising sensor for robust wearable applications. When combined with the appropriate electrical circuit this work can be further explored in electronic skin applications, detection of arterial pulse monitoring systems, human-machine interface and opens multiple avenues of widespread usage of textiles in electronics.

CRediT authorship contribution statement

Sushmitha Veeralingam: Conceptualization, Methodology, Data curation, Writing – original draft. **Abhishek Gandrothula:** Methodology, Data curation, Writing – original draft. **Sushmee Badhulika:** Conceptualization, Formal analysis, Funding acquisition, Supervision, Writing – review & editing.

Table 1
Comparison table of Tungsten Oxysulfide Coated Nylon Device with previously reported multifunctional sensors.

S. No	Material	Substrate	Fabrication Process	Functionality	Performance	Response& Recovery	Refs.
1	Ppy/Ag	PDMS	Spin-Coating	Strain and Pressure	strain g.f (≈21) and pressure sensitivity (≈0.58 kPa−1)	-	[33]
2	Carbonized cotton cloth	PDMS	Carbonization	Pressure and Strain	G.F = 15	Response time = 35ms	[34]
3	Carbon Nano capsules	PDMS	continuous stirring and evaporation.	Pressure and Strain	G.F = 15.7		[25]
4	Capacitive Sensor	Spacer fabric	Knitting	Pressure and Strain	-	Response time = 150ms	[14]
6	Polypyrrole	Silicon Rubber	Solution Casting	Strain	G.F = 1.2 - 1.7	Response time = 150ms	[16]
7	Polypyrrole	Melamine Foam	Dipping & Ultra sonicating	Breath, Pressure & Strain	G.F = 23.7 & Sensitivity = 0.002	Response time = 160ms	[15]
8	Polypyrrole/ β-FeOOH	Nylon Strip	Spin Coating	Strain	$S = 3.24\ MPa^{-1}$ G.F = 3.06	Response time = 390 - 600ms	[35]
9	Ag	PET (polyethylene-terephthalate)	Sputtering	Strain, Pressure, Temperature	$S = 1.45\ MPa^{-1}$	-	[17]
10	Tungsten Oxysulfide	Nylon	Hydrothermal	Breath, Strain & Pressure	G.F = 24.2S = 1.5 KPa^{-1}	Response = 0.2s Recovery = 0.24s	This Paper

Declaration of Competing Interest

The authors declare that they have no known competing financial interests or personal relationships that could have appeared to influence the work reported in this paper.

Data availability

Data will be made available on request.

Acknowledgments

SB acknowledges financial assistance from Department of Science and Technology (DST) India, Nano Mission grant # DST/ NM/ NT/ 2020/322.

Supplementary materials

Supplementary material associated with this article can be found, in the online version, at doi:10.1016/j.materresbull.2022.112133.

References

[1] S. Veeralingam, S. Priya, S. Badhulika, NiO nanofibers interspersed sponge based low cost, multifunctional platform for broadband UV protection, ultrasensitive strain and robust finger-tip skin inspired pressure sensor, Chemical Engineering Journal 389 (2020) 124415.
[2] S. Veeralingam, P. Sahatiya, A. Kadu, V. Mattela, S. Badhulika, Direct, one-step growth of NiSe2 on cellulose paper: a low-cost, flexible, and wearable with smartphone enabled multifunctional sensing platform for customized noninvasive personal healthcare monitoring, ACS Appl. Electron. Mater. 1 (4) (2019) 558–568.
[3] H. Li, H. Yang, E. Li, Z. Liu, K. Wei, Wearable sensors in intelligent clothing for measuring human body temperature based on optical fiber Bragg grating, Opt. Express 20 (11) (2012) 11740–11752.
[4] S. Veeralingam, S. Badhulika, Bi2S3/PVDF/Ppy-Based Freestanding, Wearable, Transient Nanomembrane for Ultrasensitive Pressure, Strain, and Temperature Sensing, ACS Appl. Bio Mater. 4 (1) (2021) 14–23.
[5] R. Yin, D. Wang, S. Zhao, Z. Lou, G. Shen, Wearable sensors-enabled human–machine interaction systems: from design to application, Adv. Funct. Mater. 31 (11) (2021), 2008936.
[6] C. Majidi, Soft-matter engineering for soft robotics, Adv. Mater. Technol. 4 (2) (2019), 1800477.
[7] H. Luo, et al., Spidroin composite biomimetic multifunctional skin with meta-structure, Adv. Mater. Technol. (2022), 2101097.
[8] K. Xu, Y. Lu, K. Takei, Multifunctional skin-inspired flexible sensor systems for wearable electronics, Adv. Mater. Technol. 4 (3) (2019), 1800628.
[9] M. Chung, G. Fortunato, N. Radacsi, Wearable flexible sweat sensors for healthcare monitoring: a review, J. R. Soc. Interface 16 (159) (2019), 20190217.
[10] S. Chen, J. Luo, X. Wang, Q. Li, L. Zhou, C. Liu, C. Feng, Fabrication and piezoresistive/piezoelectric sensing characteristics of carbon nanotube/pva/nano-zno flexible composite, Sci. Rep. 10 (1) (2020) 1–12.
[11] J. Huang, D. Li, M. Zhao, H. Ke, A. Mensah, P. Lv, Q. Wei, Flexible electrically conductive biomass-based aerogels for piezoresistive pressure/strain sensors, Chem. Eng. J. 373 (2019) 1357–1366.
[12] P. Song, B. Liu, C. Liang, K. Ruan, H. Qiu, Z. Ma, J. Gu, Lightweight, flexible cellulose-derived carbon aerogel@ reduced graphene oxide/PDMS composites with outstanding EMI shielding performances and excellent thermal conductivities, Nano Micro Lett. 13 (1) (2021) 1–17.
[13] S. Praveen, S. Veeralingam, S. Badhulika, A flexible self-powered UV photodetector and optical UV filter based on β-Bi_2O_3/SnO_2 quantum dots schottky heterojunction, Adv. Mater. Interfaces 8 (15) (2021), 2100373.
[14] B. Zhao, Z. Dong, H. Cong, A wearable and fully-textile capacitive sensor based on flat-knitted spacing fabric for human motions detection, Sens. Actuators A 340 (2022), 113558.
[15] S. Veeralingam, S. Praveen, M. Vemula, S. Badhulika, One-step synthesis of carbon doped Ppy nanoparticles interspersed 3D porous melamine foam for high performance piezoresistive pressure, strain, and breath sensor, Mater. Chem. Front. (2022).
[16] A.S. Kurian, H. Souri, V.B. Mohan, D. Bhattacharyya, Highly stretchable strain sensors based on polypyrrole-silicone rubber composites for human motion detection, Sens. Actuators A 312 (2020), 112131.
[17] X. Zhao, Q. Hua, R. Yu, Y. Zhang, C. Pan, Flexible, stretchable and wearable multifunctional sensor array as artificial electronic skin for static and dynamic strain mapping, Adv. Electron. Mater. 1 (7) (2015), 1500142.
[18] P. Sahatiya, S. Badhulika, Fabrication of a solution-processed, highly flexible few layer MoS_2 (n)–CuO (p) piezotronic diode on a paper substrate for an active analog frequency modulator and enhanced broadband photodetector, J. Mater. Chem. C 5 (44) (2017) 11436–11447.
[19] D. Braga, I. Gutiérrez Lezama, H. Berger, A.F. Morpurgo, Quantitative determination of the band gap of WS_2 with ambipolar ionic liquid-gated transistors, Nano Lett. 12 (10) (2012) 5218–5223.
[20] J. Sun, N. Lin, H. Ren, C. Tang, L. Yang, X. Zhao, Gas adsorption on MoS_2/WS_2 in-plane heterojunctions and the I–V response: a first principles study, RSC Adv. 6 (21) (2016) 17494–17503.
[21] S. Yao, Y. Zhu, Wearable multifunctional sensors using printed stretchable conductors made of silver nanowires, Nanoscale 6 (4) (2014) 2345–2352.
[22] D. Voiry, H. Yamaguchi, J. Li, R. Silva, D.C. Alves, T. Fujita, M. Chen, T. Asefa, V. B. Shenoy, G. Eda, M. Chhowalla, Enhanced catalytic activity in strained chemically exfoliated WS_2 nanosheets for hydrogen evolution, Nat. Mater. 12 (9) (2013) 850–855.
[23] S.Y. Cho, H.J. Koh, H.W. Yoo, J.S. Kim, H.T. Jung, Tunable volatile-organic-compound sensor by using Au nanoparticle incorporation on MoS_2, ACS Sens. 2 (1) (2017) 183–189.
[24] Y. Zheng, L. Sun, W. Liu, C. Wang, Z. Dai, F. Ma, Tungsten oxysulfide nanosheets for highly sensitive and selective NH_3 sensing, J. Mater. Chem. C 8 (12) (2020) 4206–4214.
[25] H. Stoyanov, P. Brochu, X. Niu, E.D. Gaspera, Q. Pei, Dielectric elastomer transducers with enhanced force output and work density, Appl. Phys. Lett. 2012 (100) (2012), 262902.
[26] C. Zetterberg, T. Öfverholm, Carpal tunnel syndrome and other wrist/hand symptoms and signs in male and female car assembly workers, Int. J. Ind. Ergon. 23 (3) (1999) 193–204.
[27] U. Tisch, I. Schlesinger, R. Ionescu, M. Nassar, N. Axelrod, D. Robertman, H. Haick, Detection of Alzheimer's and Parkinson's disease from exhaled breath using nanomaterial-based sensors, Nanomedicine 8 (1) (2013) 43–56.
[28] N. Fens, A.H. Zwinderman, M.P. van der Schee, S.B. de Nijs, E. Dijkers, A. C. Roldaan, P.J. Sterk, Exhaled breath profiling enables discrimination of chronic obstructive pulmonary disease and asthma, Am. J. Respir. Crit. Care Med. 180 (11) (2009) 1076–1082.
[29] C. Di Natale, A. Macagnano, E. Martinelli, R. Paolesse, G. D'Arcangelo, C. Roscioni, A. D'Amico, Lung cancer identification by the analysis of breath by means of an array of non-selective gas sensors, Biosens. Bioelectron. 18 (10) (2003) 1209–1218.
[30] Q. Lu, H. Chen, Y. Zeng, J. Xue, X. Cao, N. Wang, Z. Wang, Intelligent facemask based on triboelectric nanogenerator for respiratory monitoring, Nano Energy 91 (2022), 106612.
[31] S.S. Gunasekaran, S. Veeralingam, S. Badhulika, One for two" strategy of fully integrated textile based supercapacitor powering an ultra-sensitive pressure sensor for wearable applications, Journal of Energy Storage 48 (2022) 103994.
[32] S.T. Han, H. Peng, Q. Sun, S. Venkatesh, K.S. Chung, S.C. Lau, V.A.L. Roy, An overview of the development of flexible sensors, Adv. Mater. 29 (33) (2017), 1700375.
[33] D. Wang, X. Zhou, R. Song, C. Fang, Z. Wang, C. Wang, Y. Huang, Freestanding silver/polypyrrole composite film for multifunctional sensor with biomimetic micropattern for physiological signals monitoring, Chem. Eng. J. 404 (2021), 126940.
[34] C. Deng, L. Pan, R. Cui, C. Li, J. Qin, Wearable strain sensor made of carbonized cotton cloth, J. Mater. Sci. Mater. Electron. 28 (4) (2017) 3535–3541.
[35] B. Wang, K. Yang, H. Cheng, T. Ye, C. Wang, A hydrophobic conductive strip with outstanding one-dimensional stretchability for wearable heater and strain sensor, Chem. Eng. J. 404 (2021), 126393.